Materials Sciences and Applications, 2018, 9, 637-656
http://www.scirp.org/journal/msa
ISSN Online: 2153-1188
ISSN Print: 2153-117X

Structural Changes in Human Teeth after Heating up to 1200˚C in Argon Atmosphere

Nancy Vargas-Becerril, Ramiro García-García, José Reyes-Gasga*

Instituto de Física, UNAM, México City, México
Email: *jreyes@fisica.unam.mx

How to cite this paper: Vargas-Becerril, N., García-García, R. and Reyes-Gasga, J. (2018) Structural Changes in Human Teeth after Heating up to 1200˚C in Argon Atmosphere. *Materials Sciences and Applications*, **9**, 637-656.
https://doi.org/10.4236/msa.2018.97046

Received: May 18, 2018
Accepted: June 25, 2018
Published: June 28, 2018

Abstract

The phase transformation of hydroxyapatite (HAP, $Ca_{10}(PO_4)_6(OH)_2$) to the beta tricalcium phosphate phase (β-TCP, β-$Ca_3(PO_4)_2$) at 1100˚C is well known. However, in the case of human tooth, the HAP phase transformation is still an open area. For example, the CaO phase has sometimes been reported in the set of phases that make up the teeth. In this study, physical changes of human teeth when subjected to heat treatment in inert atmosphere (argon) were studied. The results were compared with those obtained in air atmosphere, from room temperature (25˚C) up to 1200˚C. Morphological changes were analyzed by light and scanning electron microscopy (SEM). The HAP to β-TCP phase transformation was followed in powder samples by X-ray diffraction (XRD) and Fourier transform infrared spectroscopy (FTIR). Heating of teeth results in the removal of organic material and structural water before the HAP to β-TCP phase transformation, the increment in hardness and the induced crystal growth. The percentage of the phases, crystal growth and lattice parameter variations as a function of temperature was quantified by Rietveld analysis. The black color was observed in dentin heated under argon atmosphere. Differences in expansivity produce fractures in dentin at 300˚C in argon and at 400˚C in air. In dentin, the coexistence of the HAP and β-TCP phases was observed after 800˚C in argon and after 600˚C in air; in enamel it was observed at 600˚C in argon compared with 400˚C in air. In general, the role played by the argon atmosphere during the thermal treatment of the teeth is to retard the processes observed in air.

Keywords

Human Tooth, Heating Treatment, Phase Transformation, SEM, X-Ray Diffraction, FTIR

1. Introduction

Enamel has a prismatic structure composed in 96% by weight of hydroxyapatite

(HAP, $Ca_{10}(PO_4)_6(OH)_2$) nanometric-sized crystals and 4% of organic material and water [1]. Dentin has a tubular structure surrounded by HAP crystals, which make up 70% by weight; the remaining 30% is water and organic material [1]. Human tooth HAP is neither pure nor stoichiometric: enamel contains Na, Mg, Cl and C ions substituting Ca^{2+}, PO_4^{3-} and OH^- ions; dentin been reported as deficient in calcium with different amounts of HPO_4^{2-} and CO_3^{2-} ions [2].

The phase transformation of HAP is well stablished, and it is done in agreement with the CaO-P_2O_5 phase diagram. It is well known that HAP transforms to the beta tricalcium phosphate phase (β-TCP, β-$Ca_3(PO_4)_2$) at 1100˚C [3]. However, the HAP in human tooth is a theme still open. For example, Brès *et al.* [4] reported the existence of crystalline and amorphous CaO when they analyzed human tooth enamel by transmission electron microscopy. CaO has also been reported in bovine teeth and bones when they are heat treated [5] [6]. The remaining question is related to the phases that would be observed when the teeth are subjected to thermal treatments and the temperature at which these phases appear.

Temperature effect on the structure of human tooth has been analyzed in air by different techniques since long ago. It is well known that when teeth are submitted to temperature in air, structural changes can be evidenced by color changes and fractures [7] [8], as well as changes hardness [9] and electrical conductivity [10]. For example, Reyes-Gasga *et al.* [11] and Tiznado-Orozco *et al.* [12] studied healthy and carious samples in the range 20˚C to 600˚C and the variations in the HAP hexagonal lattice parameters were related with ion substitution of CO_3^{2-} in the OH^- and PO_4^{3-} sites. Sandholzer *et al.* [13] heated bulk tooth samples from 400˚C to 900˚C in air and suggested that temperature produces a high degree of perfection in the crystal structure of dentin but limited in enamel. Fereira *et al.* [14] analyzed bulk tooth samples in the range 20˚C to 1150˚C and observed that teeth gradually heated in air showed minimal damage by fracture, but with fast heating dentin and enamel are abruptly separated at the enamel-dentin junction and the fracture damage is severe. In addition, Reyes-Gasga *et al.* [15] reported a dielectric-conductive transition in human tooth enamel above 250˚C in air and in vacuum.

The aim of this paper is to observe the phases and to find the differences produced by the heating treatments of the teeth done in argon atmosphere compare the results with those observed in air. Therefore, in this work bulk and powder tooth samples were subjected to temperatures in the range from room temperature (25˚C) to 1200˚C in argon and in air atmospheres. The macro and microstructure, color, and mechanical changes in enamel and dentin were analyzed as a function of temperature. The color, mechanical and structural changes of the bulk samples were analyzed through hardness variation via the micro-indentation, and the light (LM) and scanning electron (SEM) microscopies. The structural and phase changes were also analyzed in powder samples via the X-ray diffraction (XRD), thermogravimetric analysis (TGA) and its differential (dTGA) and

Fourier transform infrared spectroscopy (FTIR) analyses which were used to determine lattice parameters of crystal size, phase ratios and other crystallographic aspects using the Rietveld method.

It is worth to mention that similar studies have also been carried out in human and animal bone samples in the range 20˚C to 1200˚C to investigate the HAP structure change by heating to design materials with potential applications in odontology and medicine. For example, Rogers and Daniels [5] observed variation in the elastic modulus for temperatures above 600˚C in human bone bulk samples. Mezahi *et al.* [16] performed the calcination from 800˚C to 1200˚C of bovine bone and synthetic HAP samples and observed the formation of the β-TCP. Figuereido *et al.* [6] observed the crystal growth together decrease in porosity and formation of CaO in human, bovine and porcine bones samples. All these experiments were carried out in air. We are interested in doing the heating treatment of teeth in an inert atmosphere to have an idea of the role played by the environment where the heating takes place.

The effects of heating on the structure of the human tooth, mainly in enamel, have been minimized due to its impractical use in the dental clinic. However, exists several clinical scenarios where the temperature is increased of dental treatments (lasers, dental burrs, etc.) that authorize this study. For example, the use of the hand-piece tool in the treatment of carious teeth involves a temperature close to 200˚C [17]. Recently there has been an increase in the use of laser radiation in dental surgeries. It has been estimated, for example, that CO_2 lasers raise the temperature between 200˚C and 800˚C at the application site [18], and erbium lasers produce temperatures above 300˚C [19]. In addition, the analysis of the effects of higher temperatures on the human dental piece may play an important role in forensic research [13] [20].

2. Experimental Procedure

Dentin and enamel of thirty permanent human molars extracted for orthodontic reasons from adult patients (between 25 and 30 years old) were the working material (Institutional Review Board (IRB) approval FMED/CI/SPR/083/2015 for use of human teeth approved by the University of Mexico). This IRB approval, in accordance with the Committee on Publication Ethics (COPE) guidelines, includes written informed consent from patients about this type of study. Children's teeth were not used.

After extraction, dental pieces were rinsed with distilled water and subjected to a careful visual review using a Carl Zeiss Stemi 2000-C light stereo microscope to select only healthy pieces. They were then cut into four parts on a Buehler IsoMet 1000 diamond disk cutter. Each of them was set at temperatures ranging from 25˚C to 1200˚C at 100˚C intervals and with one hour of permanence in a Lindberg 54,233 tubular type furnace. Heating and cooling were performed slowly (10˚C/min). The experiment was carried out in argon and in air atmospheres. For heating under the argon atmosphere, the samples were heated im-

mersed in a constant argon gas flow of 0.1 ml/min that get into through one end of the tube and get out through the other. The temperature was measured with a Pt-Pt/Rh thermocouple.

For microstructure, bulk samples were observed with the Carl Zeiss Stemi 2000-C light stereo-microscope in normal reflection mode, and a FESEM JSM-6701F field emission SEM microscope with image resolution of secondary electrons of 1.0 nm for the acceleration voltage of 15 kV and of 2.2 nm for the acceleration voltage of 1 kV. For microhardness, a Matsuzawa equipment model MHT2 with a squared diamond indenter and an angle of 136˚ was used. The indentations were made using 25-gram force for 20 s. The number of indentations was 10 in each sample.

For the crystalline structure analysis, dentin and enamel were carefully mechanically separated, avoiding the zone of the amelodentinal junction to eliminate the mixing of materials. The samples were powdered using a hand dental drill and a Lynx EM-II milling cutter.

The X-ray diffraction characterization of powders was performed on a Bruker equipment model D8-Advanced with monochromatic Cu (Kα) radiation (λ = 0.154 nm). The diffractograms were obtained in the 2θ range from 5 to 60˚ with a step of 0.02˚/s, and 25 s of counting time per step using the Bragg-Brentano geometry. Computer structural analysis of diffractograms was performed by the Rietveld method using the software Profex-BGMN-Bundle-3.6.0.

The TGA analysis of the powders was performed on a TA Instrument SDT Q600 V20.9 Build 20 calorimeter from room temperature (25˚C) to 1200˚C with a heating rate of 10˚C/min, both in argon and in air. FT-IR analysis was done in the mid-infrared range 400 to 4000 cm^{-1} using a Perkin Elmer infrared spectrometer coupled with a total attenuated reflectance (ATR) of germanium.

3. Results

3.1. TGA and dTGA

Figure 1 shows the TGA and dTGA graphs of dentin in air (**Figure 1(a)**) and in argon atmosphere (**Figure 1(b)**), and of enamel in air (**Figure 1(c)**) and in argon (**Figure 1(d)**). The analysis indicates the highest percentage of weight loss occurs between 250˚C and 650˚C in dentin, and between 250˚C to 500˚C in enamel. The mean weight loss observed in dentin (34%) was greater than in enamel (23%), but the weight loss velocity is slower in argon.

In dentin, from 25˚C to 250˚C, the loss of adsorbed water and some organic material produces the weight loss of 8% in argon and 10% in air. Between 250˚C to 650˚C in argon and from 250˚C to 550˚C in air, the weight losses of 20% and 22%, respectively, are due to the loss of structural water and the total organic material removal. From 650˚C in argon and from 550˚C in air and up to 1200˚C, the weight loss of 4% in both atmospheres is due to decarbonization and dehydroxylation.

In enamel, from 25˚C to 250˚C, the weight loss of 5% is produced both in argon

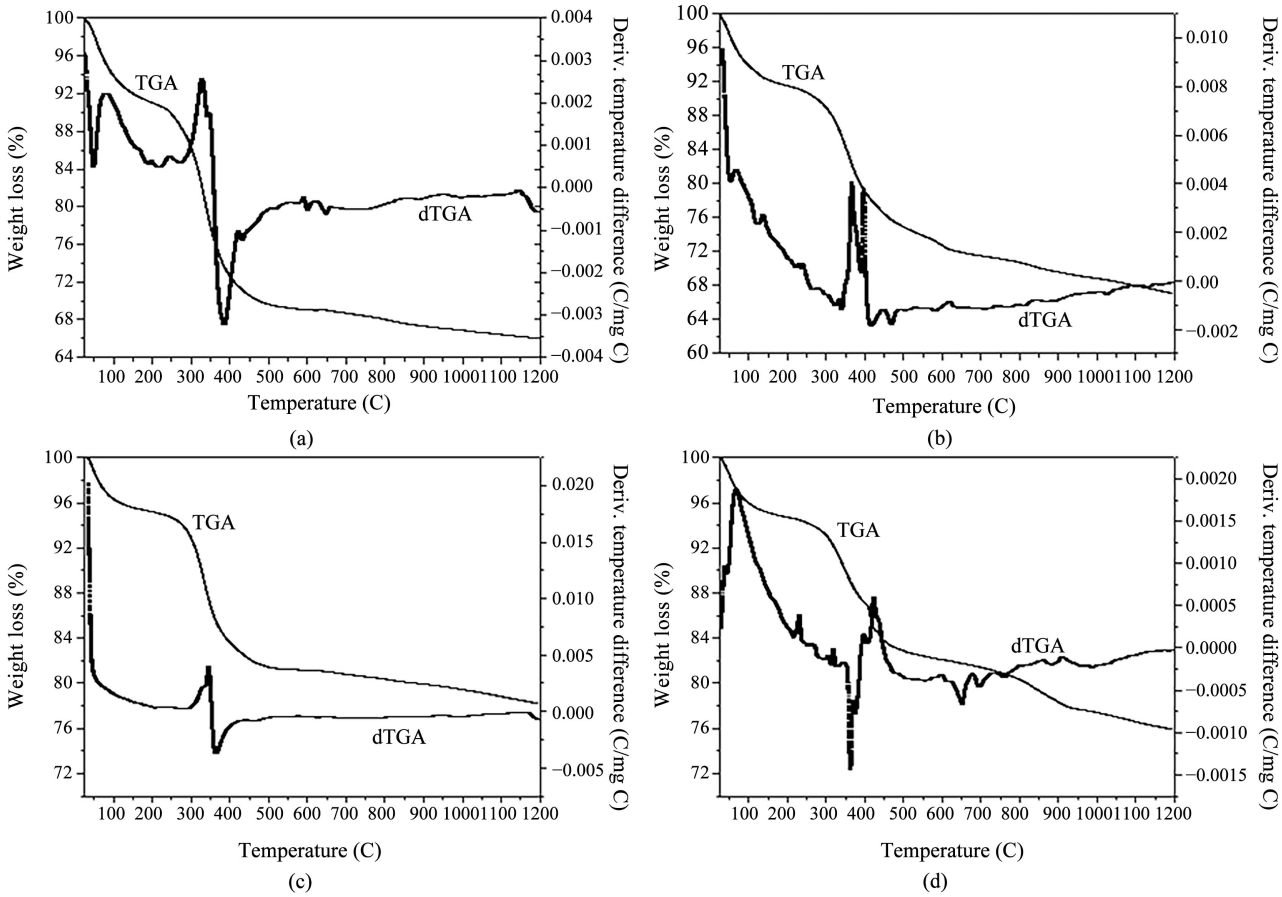

Figure 1. TGA and dTGA graphs of human tooth dentin and enamel from room temperature (25˚C) to 1200˚C. (a) Dentin in air; (b) Dentin in argon; (c) Enamel in air; (d) Enamel in argon.

and in air by the loss of adsorbed water and some organic material. From 250˚C to 450˚C in argon and from 250˚C to 500˚C in air, the weight losses of 11% and 13% respectively are produced by the elimination of structural water and the total elimination of organic material. The last weight loss registered in air is of 4% from 500˚C to 1200˚C; but in argon there are two losses: one of 6% from 450˚C to 900˚C and other of 2% from 900˚C to 1200˚C. These losses are due to decarbonization and dihydroxylation reactions.

3.2. Color Changes

The color changes in enamel are in function of temperature. **Figure 2** shows the images of the dental piece after heating in the argon atmosphere. In this case, the changes of color in dentin start from 100˚C, where it is light brown. Enamel conserves its natural color. At 200˚C, dentin changes to yellow-orange, while the enamel is bluish white. At 300˚C, dentin is gray and begins to show cracks. The enamel is light gray. At 400˚C, dentin is dark (!). Enamel is still light gray and begins to fracture, although much less than in dentin, and dentin is separated from enamel. At 600˚C, at the amelodentinal junction, dentin changes to dark gray. At 800˚C, dentin and enamel are light gray. At 900˚C, dentin is white, al-

though close to the amelodentinal junction, dentin and enamel are olive-colored. Enamel is mostly white. At 1000˚C, enamel shows large olive areas at the amelodentinal junction. At 1200˚C both enamel and dentin are white.

For comparison, Figure 3 shows the light microscopy images of the dental piece after the heat treatments in air. At 100˚C, the color and surface structure of enamel and dentin still present their natural color. At 200˚C, enamel does not change in color, but dentin is light-brown. At 300˚C dentin is brown with some areas in olive-green color. Enamel presents areas in light-brown color.

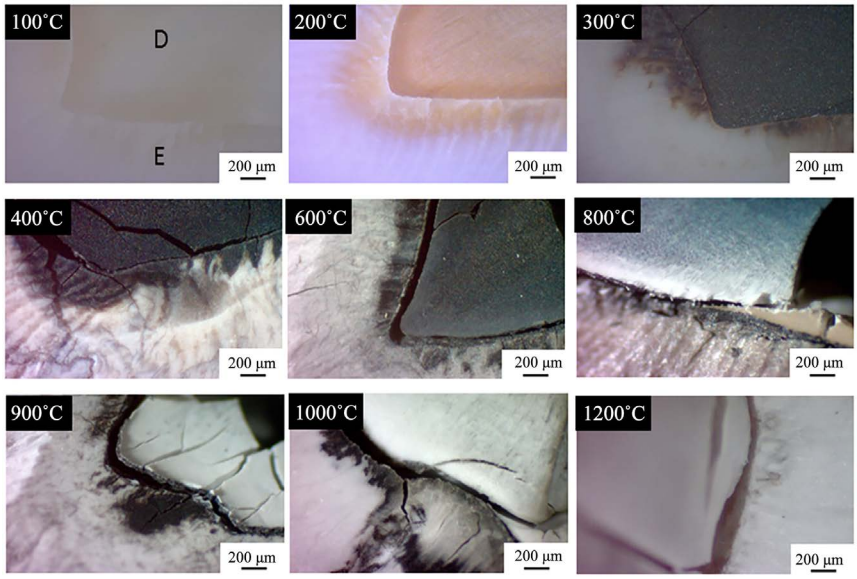

Figure 2. Light microscopy images of the dental piece after heating in argon at different temperatures. Note the color changes in each case and the occurrence of fractures in dentin after 400˚C.

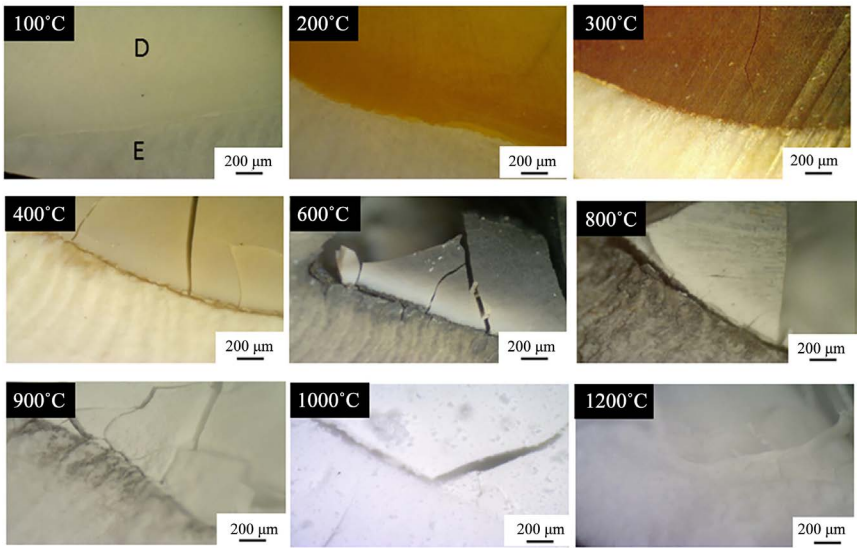

Figure 3. Light microscopy images of the dental piece after heating in air at different temperatures. Note the color changes in each case and the occurrence of fractures in the dentin after 400˚C.

At 400˚C, the amelodentinal junction shows the olive-green color, which spreads towards enamel, while dentin becomes light gray. In addition, some cracks appear in dentin, and enamel and dentin begin to separate. At 600˚C, dentin presents fractures and its color is dark gray. Enamel is dark gray, which changes to light gray towards the outside. At 800˚C, all enamel is dark gray, while dentin is light gray. At 900˚C both dentin and enamel show the same color, light gray. At 1000˚C, enamel and dentin are white. Finally, at 1200˚C, both structures display a gray white color.

Therefore, enamel follows the color sequence:

$$[\text{Natural Color}] \rightarrow [\text{Light Gray}] \rightarrow [\text{Dark Gray}] \rightarrow [\text{Light Gray}] \rightarrow [\text{White}]$$

In air, the dark gray in enamel is observed at 800˚C, while in argon it is observed at around 300˚C. The darkening of the color is due to the removal of the organic material that occurs between 200˚C and 600˚C.

The color changes in dentin in air as a function of temperature follow the sequence:

$$[\text{Natural Color}] \rightarrow [\text{Brown}] \rightarrow [\text{Gray}] \rightarrow [\text{Black}] \rightarrow [\text{Gray}] \rightarrow [\text{White}]$$

Dentin is observed in black color only in argon atmosphere, at around 300˚C. This sequence is consistent with that reported in the literature under air atmosphere [13].

3.3. Hardness

Table 1 shows the Vickers microhardness values registered in enamel and dentin as a function of temperature, in argon and in air atmospheres. The graphical presentation of the data is shown in Figure 4. The hardness in enamel lies in the range from 220 to 490 HVN, whereas in dentin it is between 65 and 530 HVN, surpassing in air the hardness recorded in the enamel at 1200˚C. Note that the standard deviation of these values is higher in enamel than in dentin.

Table 1. Vickers microhardness in enamel and dentin at different temperatures in air and argon atmospheres. Note the increase of hardness in dentin, and the variation of values in enamel.

Temperature (˚C)	Air		Argon	
	Enamel (HVN)	Dentin (HVN)	Enamel (HVN)	Dentin (HVN)
25	306 ± 20	103 ± 16	306 ± 20	103 ± 16
200	346 ± 52	101 ± 9	490 ± 62	84 ± 10
400	352 ± 79	65 ± 19	331 ± 46	80 ± 6
600	286 ± 23	69 ± 7	305 ± 56	107 ± 22
800	229 ± 49	128 ±15	459 ± 64	120 ±11
1000	371 ± 66	375 ± 52	409 ± 79	207 ± 29
1200	373 ± 83	525 ± 80	299 ± 101	322 ± 57

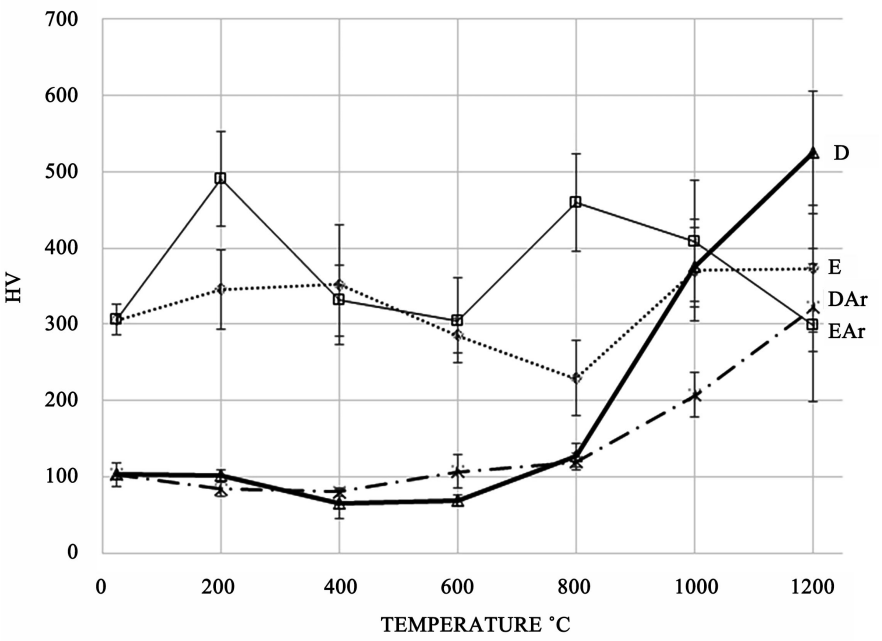

Figure 4. Vickers microhardness graph of the values presented in **Table 1** for enamel and dentin at different temperatures in air (E and D) and argon (EAr and DAr). Note the variation and the increment of the hardness in enamel and dentin respectively.

As shown in **Figure 4**, the hardness in argon of enamel is quite different than in air. In air, it shows two increments: at 200˚C, when the organic material is carbonized, and at 800˚C, when the β-TCP phase is present (as it will be commented below). The hardness in argon and in air is almost similar when the organic material is eliminated.

In dentin, the increment in hardness is observed after 200˚C in argon while it decreases in air. This is, after the elimination of the organic material. After 800˚C, the hardness increases both in air and in argon. Moreover, the hardness in dentin in air is higher than in enamel at 1200˚C.

3.4. SEM

Figure 5 shows the SEM images of dentin at different temperatures in air (**Figure 5(a)**) and in argon (**Figure 5(b)**). Note that in air, HAP dentin crystals coalesce at 200˚C, during the water and organic material losses. Coalescence of these crystals in argon is slower than in air. It begins at 200˚C; but at 600˚C the dentinal conducts are still present. After elimination of the organic material, at 800˚C, the dentinal conducts disappear. Above 1000˚C, an equiaxial granular structure is formed.

Figure 6 shows the corresponding SEM images for enamel in air (**Figure 6(a)**) and in argon (**Figure 6(b)**). The elongated HAP enamel crystals coalesce at 200˚C in argon (at 600˚C in air). After elimination of the organic material, at 600˚C, both structures show similar contrast. Above 600˚C in argon, the crystals form a molten structure, initially porous (1000˚C) and then they grow (1200˚C).

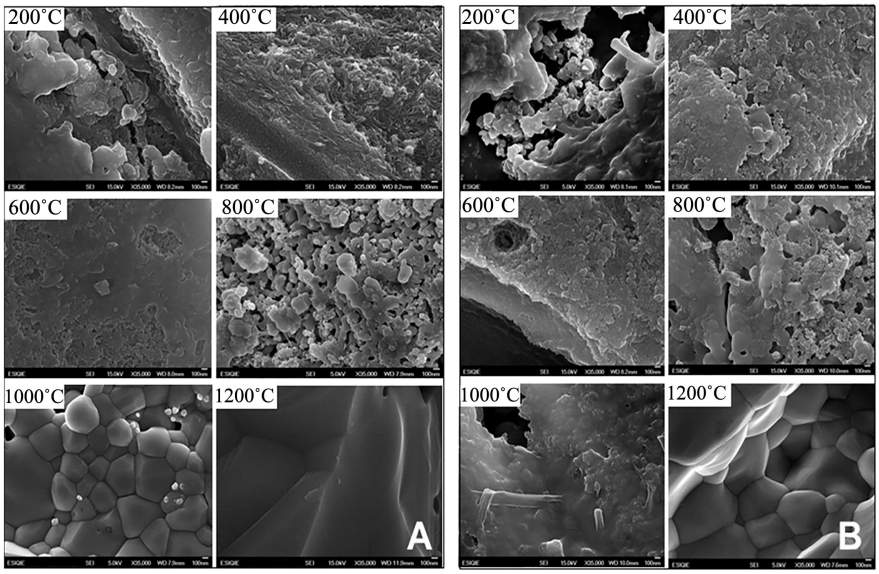

Figure 5. SEM images of dentin at different temperatures in air (A) and in argon (B).

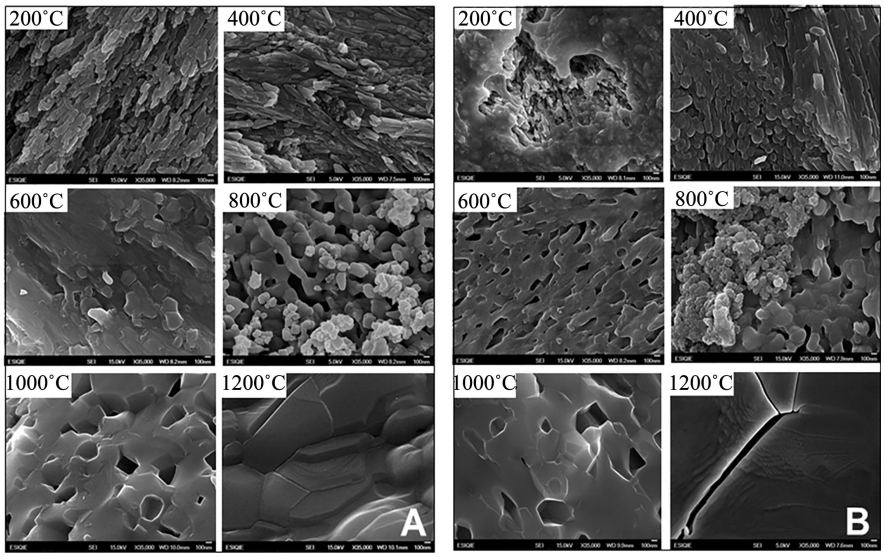

Figure 6. SEM images of enamel at different temperatures in air (A) and in argon (B).

Mezahi *et al.* [16] obtained similar results in bovine bones and synthetic HAP samples heated up to 1200˚C in air.

3.5. XRD

Figure 7 shows the XRD diffractograms of dentin (**Figure 7(a)** and **Figure 7(b)**) and enamel (**Figure 7(c)** and **Figure 7(d)**) at different temperatures in air (**Figure 7(a)** and **Figure 7(c)**) and in argon (**Figure 7(b)** and **Figure 7(d)**). For the identification of the HAP and β-TCP phases, the PDF cards No. 09-0432 and 70-2065, respectively, were used.

At room temperature, HAP is the phase identified, although in dentin it shows an "amorphous-type" spectrum when the temperature is below 400˚C

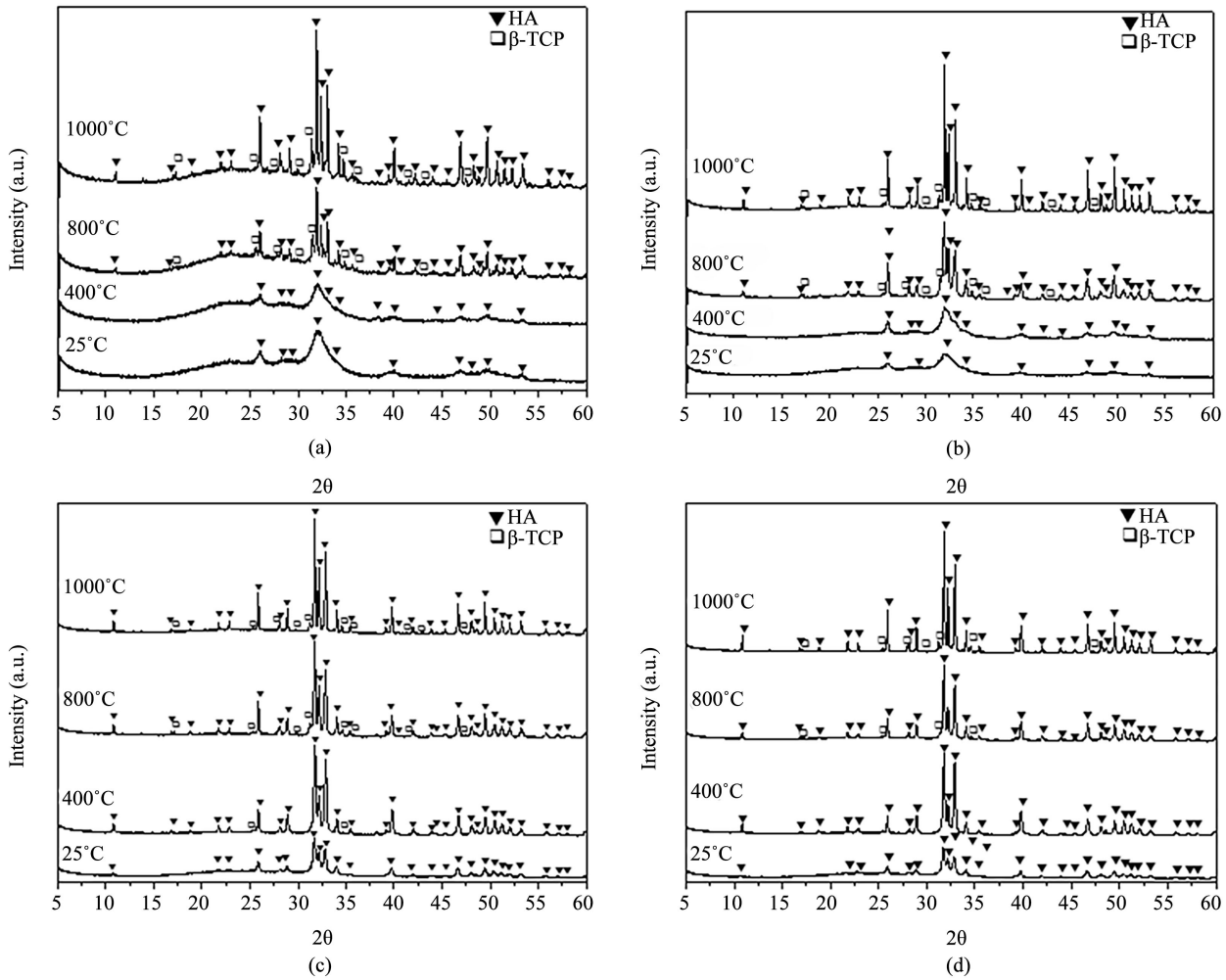

Figure 7. XRD diffractograms of dentin (a) (b) and enamel (c) (d) at different temperatures in air (a) and (c) and in argon (b) and (d).

produced by the smaller crystal size of HAP (see **Table 2**) [4]. Above 800˚C, the diffraction peaks are thinner, which indicates an increment in crystal size.

The presence of the β-TCP phase was observed after the elimination of water and organic material, and after the crystal growth of HAP. The coexistence of HAP and β-TCP, in enamel was registered at 400˚C in air and at 600˚C in argon. In dentin, it was observed at 600˚C in air and at 800˚C in argon.

3.5.1. Phase Transformation

Table 3 indicates the relative percentage of the HAP and β-TCP phases obtained by the Rietveld method from **Figure 7**. For dentin, the coexistence of the two phases is observed after 600˚C in air and after 800˚C in argon. At 1200˚C, for dentin in air the percentage is 84% HAP and 15% β-TCP, while in argon it is 72% HAP and 27% β-TCP. For enamel, the coexistence of these phases is observed after 400˚C in air and after 600˚C in the argon. At 1200˚C, the percentage is 94% HAP and 5% β-TCP in air, and 91% HAP and 8% β-TCP in argon.

Table 2. Crystal size of the HAP and β-TCP phases obtained by Rietveld analysis from the XRD diffractograms shown in **Figure 7** using the (110) and (002) for HAP and the (002) for β-TCP.

	Temperature (˚C)	Air			Argon		
		HAp		β-TCP	HAp		β-TCP
		(110) (nm)	(002) (nm)	(002) (nm)	(110) (nm)	(002) (nm)	(002) (nm)
Dentin	25	4.8 ± 0.08	11 ± 0.5	--	4.8 ± 0.1	10.8 ± 0.5	--
	200	6.5 ± 0.1	15 ± 0.6	--	6.8 ± 0.2	9.3 ± 0.3	--
	400	4 ± 0.1	3.4 ± 0.1	--	7.7 ± 0.1	18.5 ± 0.8	--
	600	6 ± 0.3	5.6 ± 0.3	55 ± 2	12 ± 0.1	19.2 ± 0.6	--
	800	56 ± 3	53 ± 4	64 ± 1	36 ± 0.9	57 ± 2	87 ± 8
	1000	98 ± 3	92 ± 4	108 ± 7	136 ± 3	145 ± 5	139 ± 18
	1200	155 ± 7	161 ± 9	98 ± 6	121 ± 5	118 ± 7	84 ± 4
Enamel	25	26 ± 0.3	28 ± 0.8	--	26 ± 0.3	28 ± 0.8	--
	200	22 ± 0.4	23 ± 0.8	--	22 ± 0.5	23 ± 0.8	--
	400	53 ± 2	56 ± 3	23 ± 4	61 ± 2	68 ± 3	--
	600	58 ± 1	69 ± 3	98 ± 11	58 ± 1	69 ± 3	98 ± 11
	800	77 ± 4	90 ± 6	57 ± 4	62 ± 2	69 ± 3	100 ± 17
	1000	129 ± 7	144 ± 11	147 ± 21	126 ± 6	150 ± 10	134 ± 12
	1200	38 ± 3	31 ± 3	54 ± 25	134 ± 7	154 ± 13	125 ± 12

Table 3. Relative percentage of the HAP and β-TCP phases obtained by the Rietveld method from the XRD diffractograms shown in **Figure 7**. The % RWP is also indicated for each case.

	Temperature (˚C)	Air			Argon		
		% Hap	% β-TCP	% R_{WP}	% HAp	% β-TCP	% R_{wp}
Dentin	25	100	--	4.45	100	--	4.45
	200	100	--	4.73	100	--	5.25
	400	100	--	4.88	100	--	5.41
	600	98.04	1.96	5.65	100	--	5.93
	800	90.71	9.29	7.95	90.91	9.09	5.99
	1000	77.98	22.02	7.4	89.94	10.52	7.63
	1200	84.15	15.85	6.42	72.58	27.42	7.31
Enamel	25	100	--	5.72	100	--	5.72
	200	100	--	5.52	100	--	4.71
	400	99.39	0.61	5.89	100	--	5.97
	600	94.88	5.12	6.35	93.67	6.33	5.72
	800	88.93	11.07	6.55	96.12	3.88	5.78
	1000	92.13	7.087	7.15	92.59	7.41	7.33
	1200	94.9	5.1	8.35	91.83	8.17	7.02

3.5.2. Crystal Size

The crystal-size values were also obtained by the Rietveld analysis. **Table 2** shows the crystal size for the HAP and β-TCP phases. In general, above 400˚C in enamel and above 600˚C in dentin and up to 1000˚C, the crystal size of both phases grows in a directly proportional relationship with temperature. At 1200˚C, in dentin in air and enamel in argon, the HAP crystals keep growing. In contrary, the crystal size decreases in dentin in argon and enamel in air. In all cases, after 1000˚C the β-TCP crystals decrease. The biggest decrement of the HAP and β-TCP crystals is observed in enamel in air.

3.5.3. Lattice Parameters

The lattice parameters were also obtained by the Rietveld analysis. **Table 4** shows the percentage of variation for the HAP (PDF card 09-0432) and β-TCP (PDF card 70-2065) phases as a function of the temperature. This percentage was obtained by:

$$\% = \frac{\text{Repoted Value} - \text{Calculated Value}}{\text{Reported Value}} \times 100$$

where the "reported values" (nominal values) were a = 0.94 nm and c = 0.688 nm for HAP and a = 10.43 nm and c = 37.375 nm for β-TCP; the "calculated value" is the one calculated by Rietveld.

Table 4. Percentage variation of the HAP and β-TCP lattice parameters obtained from the XRD diffractograms shown in **Figure 7** by Rietveld analysis.

	Temperature (˚C)	Air				Argon			
		HAp		β-TCP		HAp		β-TCP	
		Δa (%)	Δc (%)	Δa (%)	Δc (%)	Δa (%)	Δc (%)	Δa (%)	Δc (%)
Dentin	25	5.9	6.3	--	--	5.9	6.3	--	
	200	1.8	2.0	--	--	3.5	3.8	--	
	400	2.2	1.2	--	--	1.4	1.5	--	
	600	−0.1	−0.1	5.6	−0.6	0.2	0.5	--	
	800	−0.1	0.0	0.9	0.7	0.3	0.3	1.0	1.0
	1000	0.2	0.2	0.7	0.8	0.1	0.1	0.6	0.5
	1200	0.2	0.1	0.5	0.5	0.2	0.1	0.6	0.6
Enamel	25	−0.1	0.2	--	--	−0.1	0.2	--	
	200	−0.1	0.2	--	--	−0.1	0.2	--	
	400	−0.2	0.0	0.8	0.5	−0.1	0.1	--	
	600	0.0	0.2	0.9	0.9	0.0	0.2	0.9	0.9
	800	−0.1	0.2	0.7	0.7	0.0	0.2	1.0	0.7
	1000	−0.1	0.1	0.6	0.5	0.0	0.1	0.5	0.5
	1200	−0.2	0.2	0.8	0.7	−0.1	0.0	0.4	0.4

In dentin, for HAP in argon, Δa and Δc are highly expanded at 25˚C. They slowly decrease after 200˚C reaching 0.1% at 1000˚C. For β-TCP in dentin and in argon, Δa and Δc are expanded (around 1.0%) at 600˚C, and after 1000˚C both parameter present contraction (0.6%).

In dentin in air, for HAP Δa is highly expanded (5.9%) at 25˚C. It rapidly decreases after 200˚C reaching −0.1% at 600˚C, and it is expanded again but only 0.2% at 1200˚C. For β-TCP in dentin in argon, Δa presents a high variation in contraction from 5.6% at 600˚C to 0.9% at 800˚C. After this, remains in contraction until 0.5% at 1200˚C. Δc is expanded from −0.6% at 600˚C to 0.8% at 1000˚C.

Enamel in argon, the variations from their nominal values are very small. For HAP in enamel and in argon, Δa, varies from −0.1% (contraction) at 25˚C to 0.0% at 600˚C and remains there till 1200˚C. Δc varies from 0.2% (expansion) to 0.0% (contraction) at 1200˚C. For β-TCP in enamel and in argon, Δa and Δc are expanded (around 0.9%) at 600˚C, and after 1000˚C both parameter present contraction.

In enamel in air, for HAP, Δa, varies from −0.1% (contraction) at 25˚C to 0.0% (increase) at 600˚C and back to contraction (−0.2%), while Δc varies from 0.2% (expansion) at 25˚C to 0.0% (contraction) at 400˚C, and back to expansion (0.2%). For β-TCP in enamel in air, Δa and Δc remains expanded (around 0.7%).

Therefore, in dentin, the lattice parameters of HAP and β-TCP phases show contraction during heating but in argon these variations are slower than in air. In enamel, the lattice parameters show very small variations during heating, and they are very similar in argon and in air. Both materials reach their nominal lattice parameter values during heating.

3.6. FTIR

Figure 8 shows the FTIR spectra of dentin (**Figure 8(a)** and **Figure 8(b)**) and enamel (**Figure 8(c)** and **Figure 8(d)**) at different temperatures in air (**Figure 8(a)** and **Figure 8(c)**) and in argon (**Figure 8(b)** and **Figure 8(d)**). **Table 5** shows the positions of the bands and the corresponding mode of vibration. In dentin, the biggest differences are observed after 800˚C, when the β-TCP phase appears, mainly in the band at 1120 cm^{-1} (the asymmetric P-O ν_3 stretching mode of the β-TCP phase); it is not observed in argon. In enamel, this band, and the band at 946 cm^{-1}, they do not appear both in argon and in air.

The carbonate CO_3^{2-} ions may occupy two sites within the apatite structure. When they occupy the hydroxyl groups OH^- sites, HAP is a type-A carbonated apatite and an expansion in the a-axis and the contraction in the c-axis are registered [21]. The bands at 876 - 880 cm^{-1} and at 1444, 1456 - 1460 and 1546 cm^{-1} are observed [22] [23]. When they occupy the tetrahedral PO_4^{3-} sites, HAP is a carbonated apatite type-B, and the a-axis contracts and the c-axis expands [21]. Then, the band at ~875 cm^{-1}, corresponding to the ν_2 vibration, and the bands at

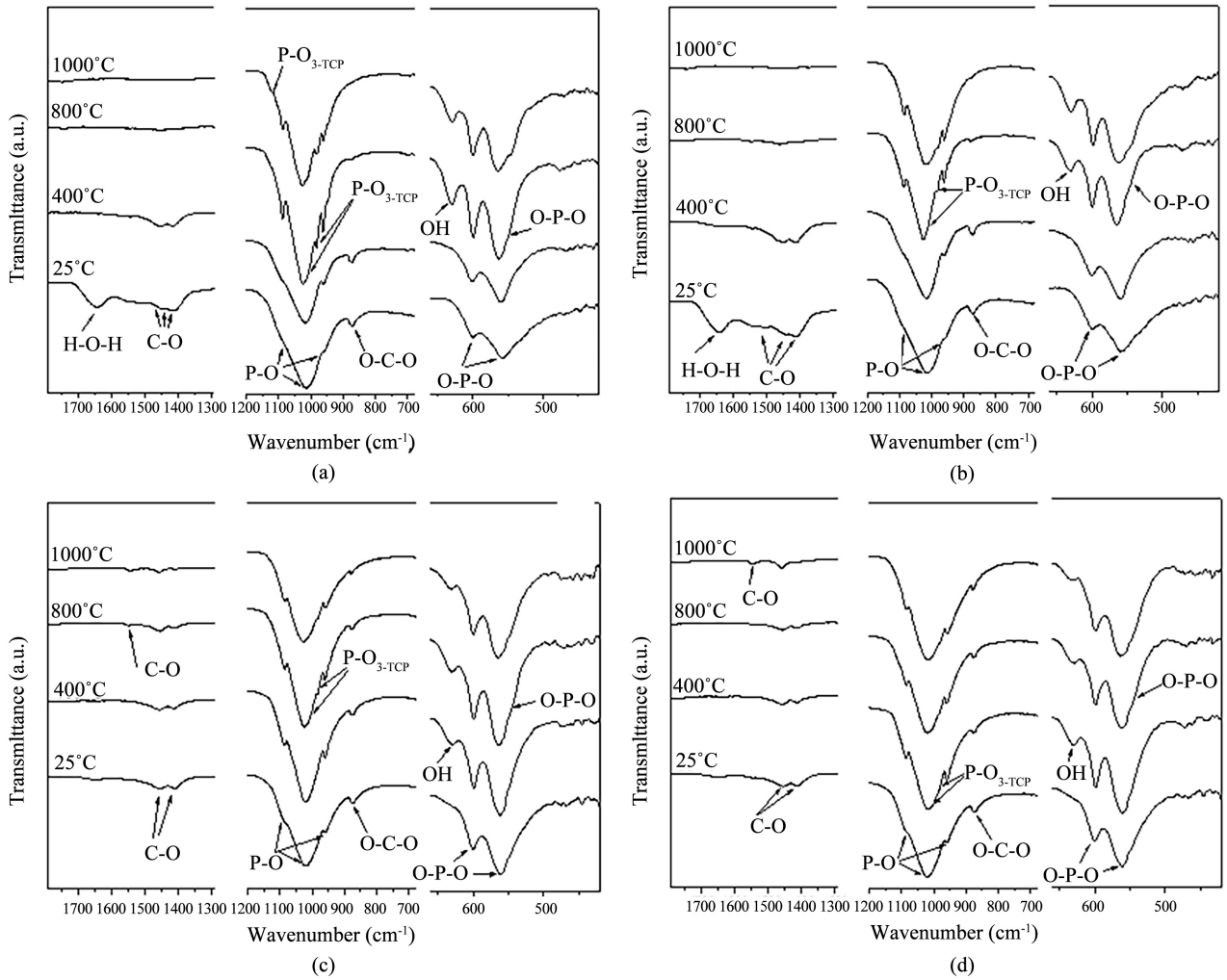

Figure 8. FTIR spectra of dentin (a) (b) and enamel (c) (d) at different temperatures in air (a) and (c) and in argon (b) and (d).

~1384, 1420, 1455 cm^{-1}, corresponding to the ν_3 stretch vibration, are observed [22] [23] The type-B apatites, also present the substitution of vacancies of oxygen in the tetrahedron and, perhaps, by molecules of water in the sites of the calcium. Vibrations at 1468 - 1470 cm^{-1} are produced by vacancies [24]. Bands at 1413, 1441 to 1470, and 1501 to 1547 cm^{-1} are assigned to the C-O asymmetric stretch vibration mode.

In dentin, amount of CO_3^{2-} eliminated in air is bigger than in argon. **Table 5** indicates that in dentin the CO_3^{2-} ions in the type-B apatite disappear around 400˚C in air and argon, while the type-A remains after 800˚C. In enamel, the type-A and the type-B apatites remains in argon at 1000˚C, but in air the type-B disappear after 800˚C.

For the phosphate group PO_4^{3-}, the bands at 1010 and 1026 cm^{-1} and at 1080 and 1088 cm^{-1}, corresponding to the ν_3 triple asymmetric degeneration vibration mode, and at 958 to 968 cm^{-1}, corresponding to the ν_1 symmetric vibration mode, are always observed both in detin and enamel and both air and argon. Also, the degenerate double bond of the ν_4 mode is in the bands at 598 and 601

Table 5. Band position assignment for the human dental tissues, enamel and dentin, from 25˚C to 1000˚C in air and in argon atmosphere. D indicates the main difference between the bands observed in the argon and air atmospheres.

Vibration	Band position (cm^{-1})															
	Dentin								Enamel							
	Air				Argon				Air				Argon			
	25˚C	400˚C	800˚C	1000˚C	25˚C	400˚C	800˚C	1000˚C	25˚C	400˚C	800˚C	1000˚C	25˚C	400˚C	800˚C	1000˚C
O-P-O ν_2	469	467	475	470	470	468	470	472	468	471	470	475	476	473	470	471
O-P-O ν_4	557 559	559 601	548 562 598	547, 564 599	557 599	559 601	564 599	545, 561 599	561 600	561 599	547 563 599	546, 564 599	560 600	560 599	561 599	561, 599
OH	-	-	630	630	-	-	631	630	-	629	629	630	-	629	629	629
O-C-O (B-type)	872	872	-	-	873	873	-	-	872	872	872	-	873	872	-D	-
O-C-O (A-type)	877	878	879	879	876	877	879	879	879	880	879	877	-D	879	876	878
P-O (β-TCP)	-	-	946	946	-	-	947	945	-	-	-	-	-	-	-	-
P-O	961	962	968	962	959	960	962	960	959	959	959	958	958	959	958	958
P-O ν_3 (β-TCP)	-	-	982	982	-	-	985	982	-	-	982	982	-	-	982	980
P-O ν_3 (β-TCP)	-	-	1014	1014	-	-	-D	1012	-	-D	1015	1015	-	1015	1012	1013
P-O ν_3	1010	1014 10,180	1024 1087	1025 1088	1013	-D	1026 1088	1017 1088	1019 1081	1020 1085	1024 1085	1026, 1085	1022 1082	1020 1086	1020 1085	1017 1085
P-O ν_3 (β-TCP)	-	-	1120	1120	-	-	-D	-D	-	-	-	-	-	-	-	-
C-O	(B)1411 (A)1444 (V)1467	(B)1413 (B)1415 (V)1470	D-	-	(B)1412 (A)1441 (V)1468	(B)1412 (A)1447 1501 1538	(A)1460 (A)1541	-	(B)1411 (A)1452	(B)1413 (A)1454	(B)1411 (A)1456 (A)1547	(A)1456 (A)1545	(B)1409 (A)1454	(B)1411 (A)1456	(B)1411 (A)1456	(B)1413 (A)1459 (A)1545

and 544 to 564 cm^{-1} of the O-P-O bond, and the bands located between 463 and 475 cm^{-1} of the ν_2 vibration mode, are always shown.

Therefore, at room temperature, HAP in dentin and enamel is a carbonated-HAP, with carbonate at sites A and B. As temperature increases, carbonates move from sites B to sites A, producing the contraction of the a-axis. At the same time, Table 4 indicates that the parameter variation is no longer so significant, possibly because the number of carbonates is lower.

4. Discussion

The differences observed under argon and under air are better described if the heating process is divided into two parts: before and after the elimination of the organic material that takes place around 600˚C. In the first part, during the eliminating the water and organic material, all the combustion reactions are favored by the oxidizing atmosphere in air, and, at the same time, the resulted heat

is dissipated. In argon, the chemical reactions are completely entrained by the argon environment and the heat dissipation is reduced [6] [25] [26]. After 600˚C, there is growth of the HAP crystals and the phase transformation to β-TCP phase.

The argon atmosphere produces slightly different color changes as compared to those in air due to argon does not react with the organic material and the residues are trapped. This explain the black color of dentin that was observed in only under argon atmosphere. Cracking and fracture of dentin are the result of the difference in expansibility, that is more severe in argon than in air.

The variation in the lattice parameters at the beginning and during heating, both in air and in argon, is greater in dentin than in enamel. In dentin, the a- and c-axes decrease 6% approximately. In enamel, the variation ranges from 0.2% to −0.1% during all heating. A simple explanation of these variations is not easy, although, they should be associated with the movement of CO_3 ions within the crystal structure of the HAP [27] [28] [29] and by the removal of the organic material, structural water, carbonates and phase transformation. However, except for the PO_4^{3-} ion, no simple ion substitution mechanism can consider the magnitude and direction of the observed parameter changes, especially when the movement of organic material and water is also present.

After the combustion of the organic components, removal of water and carbonates, the increment of hardness in dentin must have to do with the crystal growth. The particle size is reduced by the nucleation and growth of the β-TCP phase, producing a kind of composite material increasing hardness.

Note that CaO was not observed. Analyzing the decomposition of HAP, Savino *et al.* [30] indicated that processes of dehydroxylation in Ca-deficient apatites start at about 500˚C, while Shi *et al.* [31] ensured that in dental enamel the β-TCP phase appears above 700˚C. They also indicated that the β-TCP phase appears because of dehydration and decarbonization, producing stoichiometric HAP in dental enamel.

The chemical reactions in air for the Ca-deficient HAP by dehydroxylation are:

$$\mathrm{Ca_{10}(PO_4)_6(H_2O)_2} \rightarrow \mathrm{Ca_{10}(PO_4)(OH)_{2-2x}O_x\square_x} + x\mathrm{H_2O}$$

$$\mathrm{Ca_{10}(PO_4)_6(OH)_{2-2x}O_x\square_x} \rightarrow \mathrm{Ca_{10}(PO_4)_6O} + (1-x)\mathrm{H_2O}$$

where □ are hydrogen vacancies, $Ca_{10}(\mathrm{PO_4})_6(\mathrm{OH})_{2-2x}\mathrm{O}_x\square_x$ is oxyhydroxyapatite (OHA), and $Ca_{10}(\mathrm{PO_4})_6\mathrm{O}$ is oxyapatite (OA). For the Ca-deficient HAP to β-TCP occurring between 700˚C and 800˚C the reaction is:

$$\mathrm{Ca_{10-x}(HPO_4)_x(PO_4)_{6-x}(H_2O)_{2-x}}$$
$$\rightarrow (1-x)\mathrm{Ca_{10}(PO_4)(H_2O)_2} + 3x\beta\text{-}\mathrm{Ca_3(PO_4)_2} + x\mathrm{H_2O}$$

The argon atmosphere affects the temperature at which the β-TCP phase is observed because in air, by being an oxidizing atmosphere, it interacts with the material forming oxides and releasing the β-TCP phase. The decomposition

reactions need a greater amount of heat.

The content of β-TCP phase is higher in dentin. This could be since the crystal size in dentin is smaller than in enamel, resulting in the increase in surface energy which favors the decrease of the activation energy that the formation of this phase needs, even when this transformation starts after 600˚C.

The temperature effect on the crystal size and morphology of the enamel and dentin grains during the heat treatment of human tooth will be analyzed by electron transmission microscopy. We are working on it.

5. Conclusion

Heating of teeth in air and in argon atmospheres presents significant structural and chemical changes; the CaO was not observed. The heating analysis becomes simple if the process is divided in two parts: those occurring before and after the water and organic removal (600˚C, approximately). During the removal of the organic material and structural water the air atmosphere play an important role in the reaction of the combustion products. The appearance of the β-TCP phase depends on the temperature, the atmosphere and the chemical composition. During the phase transformation to β-TCP, the air atmosphere is important in the heat dissipation process, both in dentin and in enamel. In addition to this, the removal of organic material and of the structural water content modifies significantly the lattice parameters, mainly in the dentin. The lattice parameter variations are slower in argon than in air. The phase transformation induces hardness, mainly in dentin, and the hardness increment is accompanied by crystal growth. Therefore, there is difference between the results obtained in the heating treatment of the teeth done in air than those obtained from the heating done in argon atmosphere. In general, the argon atmosphere delays the process observed in air. Because oxidation is important, similar behavior as those in argon can be expected in vacuum.

Acknowledgements

We thank to J. Barreto Rentería, S. Tehuacanero Nuñez, R. Trejo Luna, A. Gómez Cortés, A. Morales Espino, M. Aguilar Franco, D. Quiterio, C. Zorrilla Cangas, M. Moreno Ríos and S. Tehuacanero Cuapa for the technical support. We also thank Dr. Ivet Gil-Chavarría for the Institutional Review Board (IRB) approval FMED/CI/SPR/083/2015 for use of human teeth approved by the University of Mexico (Red Conacyt Ciencia Forense). We also thank to DGAPA-UNAM for financial support through the project PAPIIT No. IN-109516. NVB thanks the CONACYT for the economic support to perform a postdoctoral stay at the Instituto de Física, UNAM.

References

[1] Le Geros, R.Z. (1991) Calcium Phosphates. In: Myers, H.M., Ed., Monographs in Oral Biology and Medicine, Karger, San Francisco.

[2] Shahmoradi, M., Bertassoni, L.E., Elfallah, H.M. and Swain, M. (2014) Fundamental

Structure and Properties of Enamel, Dentin and Cementum. In: Ben-Nissan, B., Ed., *Advances in Calcium Phosphate Biomaterials*, Vol. 2, *Springer Series in Biomaterials Science and Engineering*, Springer Science and Business, London. https://doi.org/10.1007/978-3-642-53980-0_17

[3] Skinner, H.C.W. (1974) Studies in the Basic Mineralizing System, $CaO-P_2O_5-H_2O$. *Calcified Tissue Research*, **14**, 3-14. https://doi.org/10.1007/BF02060279

[4] Brès, E.F., Moebus, G., Kleebe, H.J., Pourroy, G., Werkmann, J. and Ehret, G. (1993) High Resolution Electron Microscopy Study of Amorphous Calcium Phosphates. *Journal of Crystal Growth*, **129**, 149-162. https://doi.org/10.1016/0022-0248(93)90444-2

[5] Rogers, K.D. and Daniels, P. (2002) An x-Ray Diffraction Study of the Effects of Heat Treatment on Bone Mineral Microstructure. *Biomaterials*, **23**, 2577-2585. https://doi.org/10.1016/S0142-9612(01)00395-7

[6] Figueiredo, M., Fernando, A., Martins, G., Freitas, J., Judas, F. and Figueiredo, H. (2010) Effect of the Calcination Temperature on the Composition and Microstructure of Hydroxyapatite Derived from Human and Animal Bone. *Ceramics International*, **36**, 2383-2393. https://doi.org/10.1016/j.ceramint.2010.07.016

[7] Bachmann, L., Sena, E.T., Stolf, S.F. and Zezell, D.M. (2004) Dental Discoloration after Thermal Treatment. *Archives of Oral Biology*, **49**, 233-238. https://doi.org/10.1016/j.archoralbio.2003.08.005

[8] Karkhanis, S., Ball, J. and Franklin, D. (2009) Macroscopic and Microscopic Changes in Incinerated Deciduous Teeth. *The Journal of Forensic Odonto-Stomatology*, **27**, 9-19.

[9] Cuy, J.L., Mann, A.B., Livi, K.J., Teaford, M.F. and Weihs, T.P. (2002) Nanoindentation Mapping of the Mechanical Properties of Human Molar Tooth Enamel. *Archives of Oral Biology*, **47**, 281-291. https://doi.org/10.1016/S0003-9969(02)00006-7

[10] Eissa, M.F., El-Shamy, H.M. and Hanafy, H.S. (2012) Structural and Dielectric Properties of Sterilized Human Teeth. *Physics International*, **3**, 22-27. https://doi.org/10.3844/pisp.2012.22.27

[11] Reyes-Gasga, J., García-García, R., Arellano-Jiménez, M.J., Sanchez-Pastenes, E., Tiznado-Orozco, G.E., Gil-Chavarría, I.M. and Gómez-Gasga, G. (2008) Structural and Thermal Behaviour of Human Tooth and Three Synthetic Hydroxyapatites from 20 to 600˚C. *Journal of Physics D*: *Applied Physics*, **41**, Article ID: 225407.

[12] Tiznado-Orozco, G.E., García-García, R. and Reyes-Gasga, J. (2009) Structural and Thermal Behavior of Carious and Sound Powders of Human Tooth Enamel and Dentin. *Journal of Physics D*: *Applied Physics*, **42**, Article ID: 235408.

[13] Sandholzer, M.A., Sui, T., Korsunsky, A.M., Walmsley, A.D., Lumley P.J. and Landini, G. (2014) X-Ray Scattering Evaluation of Ultrastructural Changes in Human Dental Tissues with Thermal Treatment. *Journal of Forensic Sciences*, **59**, 769-774. https://doi.org/10.1111/1556-4029.12400

[14] Fereira, J.L., Espina de Fereira, A. and Ortega, A.I. (2008) Methods for the Analysis of Hard Dental Tissues Exposed to High Temperatures. *Forensic Science International*, **178**, 119-124. https://doi.org/10.1016/j.forsciint.2007.12.009

[15] Reyes-Gasga, J., García-García, R., Álvarez-Fregoso, O., Chavez-Carvayar, J.A. and Vargas-Ulloa, L.E. (1999) Conductivity in Human Tooth Enamel. *Journal of Materials Science*, **34**, 2183-2188. https://doi.org/10.1023/A:1004540617013

[16] Mezahi, F.Z., Oudadesse, H., Harabi, A., Lucas-Girot, A., Le Gal, Y., Chaair, H. and Cathelineau, G. (2009) Dissolution Kinetic and Structural Behaviour of Natural Hydroxyapatite vs Thermal Treatment, Comparison to Synthetic Hydroxyapatite.

Journal of Thermal Analysis and Calorimetry, **95**, 21-29.
https://doi.org/10.1007/s10973-008-9065-4

[17] Hillery, M. and Shuaib, I. (1999) Temperature Effects in the Drilling of Human and Bovine Bone. *Journal of Materials Processing Technology*, **92-93**, 302-308.
https://doi.org/10.1016/S0924-0136(99)00155-7

[18] Yilbas, B.S., Yilbas, Z. and Sami, M. (1996) Thermal Processes Taking Place in the Bone during CO_2 Laser Irradiation. *Optics & Laser Technology*, **28**, 513-519.
https://doi.org/10.1016/S0030-3992(96)00006-0

[19] Pratisto, H., Frenz, M., Ith, M., Romano, V., Felix, D., Grossenbacher, R., Altermatt, H. and Weber, H. (1996) Temperature and Pressure Effects During Erbium Laser Stapedotomy. *Lasers in Surgery and Medicine*, **18**, 100-108.
https://doi.org/10.1002/(SICI)1096-9101(1996)18:1<100::AID-LSM14>3.0.CO;2-D

[20] Holden, J.L., Clement, J.G. and Phakey, P.P. (1995) Age and Temperature Changes to the Structure and Composition of Human Bone Mineral. *Journal of Bone and Mineral Research*, **10**, 1400-1409. https://doi.org/10.1002/jbmr.5650100918

[21] Ren, F.Z., Leng, Y. and Lu, X. (2013) *Ab Initio* Simulations on the Carbonated Apatite Structure. *Key Engineering Materials*, **529-530**, 1-6.
https://doi.org/10.4028/www.scientific.net/KEM.529-530.1

[22] Zhou, W.Y., Wang, M., Cheung, W.L., Guo, B.C. and Jia, D.M. (2008) Synthesis of Carbonated Hydroxyapatite Nanospheres through Nanoemulsion. *Journal of Materials Science*: *Materials in Medicine*, **19**, 103-110.
https://doi.org/10.1007/s10856-007-3156-9

[23] Ibrahim, D.M., Mostafa, A. and Korowash, S.I. (2011) Chemical Characterization of Some Substituted Hydroxyapatites. *Chemistry Central Journal*, **5**, 74-84.
https://doi.org/10.1186/1752-153X-5-74

[24] Ivanova, T.I., Frank-Kamenetskaya, O.V., Kol'tsov, A.B. and Ugolkov, V.L. (2001) Crystal Structure of Calcium-Deficient Carbonated Hydroxyapatite Thermal Decomposition. *Journal of Solid State Chemistry*, **160**, 340-349.
https://doi.org/10.1006/jssc.2000.9238

[25] Sofronia, A.M., Baies, R., Anghel, E.M., Marinescu, C.A. and Tanasescu, S. (2014) Thermal and Structural Characterization of Synthetic and Natural Nanocrystalline Hydroxyapatite. *Materials Science and Engineering*: *C*, **43**, 153-163.
https://doi.org/10.1016/j.msec.2014.07.023

[26] Kohutová, A., Honcová, P., Svoboda, L., Bezdicka, P. and Mariková, M. (2012) Structural Characterization and Thermal Behaviour of Biological Hydroxyapatite. *Journal of Thermal Analysis and Calorimetry*, **108**, 163-170.
https://doi.org/10.1007/s10973-011-1942-6

[27] Feki, H.E., Savariault, J.M. and Salah, A.B. (1999) Structure Refinements by the Rietveld Method of Partially Substituted Hydroxyapatite: $Ca_9Na_{0.5}(PO_4)_{4.5}(CO_3)_{1.5}(OH)_2$. *Journal of Alloys and Compounds*, **287**, 114-120.
https://doi.org/10.1016/S0925-8388(99)00070-5

[28] Kee, C.C., Ismail, H. and Noor, A.F.M. (2013) Effect of Synthesis Technique and Carbonate Content on the Crystallinity and Morphology of Carbonated Hydroxyapatite. *Journal of Materials Science & Technology*, **29**, 761-764.
https://doi.org/10.1016/j.jmst.2013.05.016

[29] Kubota, T., Nakamura, A., Toyoura, K. and Matsunaga, K. (2014) The Effect of Chemical Potential on the Thermodynamic Stability of Carbonate Ions in Hydroxyapatite. *Acta Biomaterialia*, **10**, 3716-3722.
https://doi.org/10.1016/j.actbio.2014.05.007

[30] Savino, K. and Yates, M.Z. (2015) Thermal Stability of Electrochemical-Hydrothermal Hydroxyapatite Coatings. *Ceramics International*, **41**, 8568-8577. https://doi.org/10.1016/j.ceramint.2015.03.065

[31] Shi, J., Klocke, A., Zhang, M. and Bismayer, U. (2005) Thermally-Induced Structural Modification of Dental Enamel Apatite: Decomposition and Transformation of Carbonate Groups. *European Journal of Mineralogy*, **17**, 769-776. https://doi.org/10.1127/0935-1221/2005/0017-0769